buildings

MDPI

Article

Efficiency of Stochastic Finite Element Random Fields and Variables to Predict Shear Strength of Fiber-Reinforced Concrete Beams Without Stirrups

Maria Ghannoum [1], Lara Shamoun [1], Dana Nasr [1], Joseph J. Assaad [1,*], Hassen Riahi [2] and Jamal Khatib [3,*]

[1] Department of Civil and Environmental Engineering, University of Balamand, Tripoli P.O. Box 100, Lebanon; maria.ghannoum@balamand.edu.lb (M.G.); lara.shamoun@std.balamand.edu.lb (L.S.); dana.nasr@balamand.edu.lb (D.N.)
[2] Laboratoire Angevin de Recherche en Ingenierie des Systemes, University of Angers, F-49000 Angers, France; hassen.riahi@univ-angers.fr
[3] Department of Civil Engineering, Beirut Arab University, Beirut P.O. Box 11-5020, Lebanon
* Correspondence: joseph.assaad@balamand.edu.lb (J.J.A.); j.khatib@bau.edu.lb (J.K.)

Abstract: Fibers are widely used in concrete structures to control crack propagation and widening due to sustained or impact loads. Nevertheless, the concrete's mechanical and structural properties are strongly affected by the fibers' spatial distribution and clumping tendency within the mass material. The main objective of this paper is to assess the efficiency of stochastic finite element modeling to predict the shear strength properties of fiber-reinforced concrete (FRC) beams without stirrups, as tested by four-point loading. Polypropylene and polyvinyl alcohol micro-filament fibers are investigated in this experimental program at relatively high rates, varying from 0.5% to 1% by volume. A stochastic sensitivity analysis is performed using both random fields and random variables to determine the effect of fiber additions on the concrete's mechanical properties (i.e., splitting tensile strength and modulus of elasticity) including the beam cracking patterns, ductility, mid-span deflection, and ultimate load. Such data could be of interest to civil engineers and structural designers to reduce the effort and resources needed to assess the FRC strength variability and failure behaviors of structural members.

Keywords: fiber-reinforced concrete; stochastic finite element; polypropylene; polyvinyl alcohol; shear strength; beams

check for updates

Academic Editor: Grzegorz Ludwik Golewski

Received: 30 January 2025
Revised: 13 February 2025
Accepted: 19 February 2025
Published: 24 February 2025

Citation: Ghannoum, M.; Shamoun, L.; Nasr, D.; Assaad, J.J.; Riahi, H.; Khatib, J. Efficiency of Stochastic Finite Element Random Fields and Variables to Predict Shear Strength of Fiber-Reinforced Concrete Beams Without Stirrups. *Buildings* **2025**, *15*, 721. https://doi.org/10.3390/buildings15050721

Copyright: © 2025 by the authors. Licensee MDPI, Basel, Switzerland. This article is an open access article distributed under the terms and conditions of the Creative Commons Attribution (CC BY) license (https://creativecommons.org/licenses/by/4.0/).

1. Introduction

Concrete is a brittle material that is highly susceptible to crack development and tensile failure under sustained or impact loads. Currently, fibers are widely utilized to create so-called fiber reinforced concrete (FRC), possessing superior tensile strength, toughness, and load-carrying capacity [1,2]. ASTM C1116/C1116M [3] outlines four types of fibers including steel, synthetic (e.g., polypropylene (PP), polyvinyl alcohol (PVA)), alkali-resistant glass, and natural. Concrete mixtures containing PP fibers showed significantly improved strain capacity, crack control, and resistance to fire-induced spalling, making them particularly suitable for precast and industrial applications [4–9]. The incorporation of 0.1% to 0.5% of PP fibers by volume, can improve tensile and flexural strengths by 10% to 35% [10–12]. PVA fibers have found wide acceptance in engineered cementitious composites, given their strong bridging effect, emanating from both chemical and frictional bonding with the cement matrix. Li et al. [13] reported that the micro-mechanic bridging effects can be maximized using 2% PVA additions, leading to improved ductility and

strain-hardening, that could reach 7% in tension. Meng et al. [14] and Said and Razak [15] showed that PVA fibers significantly enhanced the flexural behavior of structural beams and resistance to seismic forces, including the load capacity and energy absorption in the beam–column joint zones [13,16–18].

Nonlinear finite element (FE) modeling and analysis offer efficient alternatives to simulate the behavior of structural reinforced concrete (RC) members, while reducing the difficulty and resources required for experimental testing [19–22]. Currently, the existing analytical and numerical constitutive models have mainly focused on mixtures containing steel fibers, given their rigid nature (i.e., unlike synthetic fibers) that can be replicated during the modeling process [21,23,24]. For instance, Gontero [23] developed a model that treats the steel fibers as short bars with cylindrical and straight shapes, while their inclination with respect to the loading direction can be pre-determined during the FE modeling. A four-point bending test incorporating an electromagnetic method for measuring the fiber volumetric density and orientation was performed. The model was supported with material data in the form of fields, demonstrating its ability to replicate the beam's behavior at the local scale in terms of cracking, and at the global scale in terms of force-deflection. Khan et al. [25] evaluated experimentally and numerically the cracking behavior of concrete slabs under flexural loading. Steel and PP fibers ranging from 0.7% to 1.0% and from 0.1% to 0.9%, respectively, by volume were used. The authors reported that hybrid FRC made with 0.9% steel and 0.1% PP fibers exhibited the best performance in terms of crack control, load capacity, and ductility. The proposed FE model showed a close agreement with the experimental outcomes. Huo et al. [26] developed a constitutive model that accounts for the effect of steel fiber content, spacing, and orientation in FRC mixtures. The FE simulation confirmed that the proposed constitutive model is efficient for predicting and analyzing tensile and flexural strengths.

It is important to note that most FE modeling uses deterministic approaches, wherein concrete properties are considered constant and evenly distributed throughout the structural member. This assumption, however, is unrealistic, especially in the case of FRC mixtures, in which crack initiation and propagation are strongly affected by the fibers' spatial distribution, including their clumping and balling tendencies during the mixing process [27,28]. In fact, earlier studies showed that FRC's mechanical and structural properties are characterized by large coefficients of variation, compared to fiber-free conventional concrete. For example, Buratti et al. [27] reported that the statistical variability in residual strengths of FRC mixtures containing steel and macro-synthetic fibers could reach 15% to 20%. Higher variability in the range of 10% to 33% was reported by Soetens and Matthys [29]. Glodkowska and Bury [30] concluded that the variability induced by fiber additions in compressive and tensile strength testing could reach 30%, which may result in a significant overdesign of structural members subjected to flexural loading.

Unlike the deterministic approach, stochastic FE approaches have proved efficient in appropriately modeling the behavior of heterogeneous materials, including FRC [31–34]. In addition to the presence of fibers that could alter the spatial mechanical properties, concrete's heterogeneity could also be attributed to changes in material properties, as well as to external factors such as variations in pouring and curing conditions [32,35]. Various methods have been developed for stochastic analysis. A straightforward approach involves representing uncertainties through a set of correlated random variables, wherein the variables are generated based on statistical distributions (e.g., normal, log-normal, and uniform) that represent the uncertainty of the selected mechanical property [36,37]. For example, Abbas [36] analyzed different shear strength design equations for FRC beams using the FE method, and reliability techniques by considering random variables on the geometry of the beam, reinforcement, and fibers density. A more advanced technique

incorporates the spatial variability of material or geometric properties using a continuous representation (rather than being fixed), which is known as random field [38,39]. This method requires sufficient refinement to capture variability in the random field without excessively increasing the computational costs. For instance, Zhang et al. [40] developed a three-dimensional FE model for FRC structures by simulating the heterogeneity of mortar using Weibull random fields to represent the variability properties. Specific probability density functions are used to describe the random orientation of fibers within the mortar, while orientation-dependent bond-slip models are implemented to simulate the fiber–mortar interactions.

2. Context and Paper Objectives

A limited number of investigations have assessed the efficiency of FE modelling to predict the structural behavior of FRC mixtures containing PP or PVA fibers. These types of synthetic fibers are expected to yield higher concrete variability compared to steel fibers, making it essential to develop a suitable constitutive model that best approximates the actual results obtained from experimental testing. Hence, the main objective of this paper is to assess the efficiency of two-dimensional FE modeling to predict the structural properties of FRC beams without stirrups, while accounting for strength variability induced by PP or PVA fiber additions. Such data could be of interest to civil engineers and consultants seeking to predict the effect of FRC variability due to fiber additions on the failure patterns and performance of structural members, while reducing the time and resources needed to perform experimental testing.

The paper is divided into three main parts; the first part summarizes the materials used and experimental program executed to determine FRC's mechanical properties and the shear strength of beams tested under four-point loading. PP and PVA micro-filament fibers are incorporated at relatively high rates (i.e., 0.5% to 1% by volume) to significantly alter the concrete behavior. The second part presents the deterministic FE approach and highlights the limitations associated with considering FRC properties as constant during the modeling process. The third part discusses the sensitivity of the stochastic FE approach to assess the spatial correlation between the FRC mechanical properties (i.e., splitting tensile strength and modulus of elasticity) and the cracking behavior and damage thresholds of experimental beams. The analysis is generated using both random variables (i.e., based on statistical distributions representing the uncertainty of responses) and random fields (i.e., based on random heterogeneity changes within the mass material).

3. Experimental Evaluation of Shear Strength of RC Beams Without Stirrups

3.1. Concrete Materials and Mechanical Properties

A moderate-strength concrete mix used in residential applications is considered in this work [41]; it contains 450 kg/m^3 limestone cement (GU-L) in a water-to-cement ratio of 0.47. The fine and coarse aggregate contents were 930 and 760 kg/m^3, respectively. A naphthalene-based superplasticizer (i.e., HRWR) complying with ASTM C494 Type F was employed. It had specific gravity and solid contents of 1.2 and 40%, respectively, with a maximum recommended dose of 4% by mass of cement. The HRWR was adjusted to secure fixed slump of 180 $\pm$ 20 mm.

Two types of fibers including polypropylene (PP) and polyvinyl alcohol (PVA) are used. The PP fibers had a length, diameter, and tensile strength of 12 mm, 0.03 mm, and 350 MPa, respectively, while those values were 8 mm, 0.038 mm, and 1100 MPa for the PVA fibers. The density values for the PP and PVA fibers are 910 and 1300 kg/m^3, respectively. The fibers are incorporated at relatively high rates in order to significantly alter the concrete's mechanical properties and assess the suitability of random field and random variable

generations in finite elements. to predict the shear strength of RC beams without stirrups. Hence, the PP fibers were added at two rates, of 0.5% and 0.85%, while the PVA fibers were added at 1% by volume. As summarized in Table 1, the HRWR demand increased remarkably with fiber additions, which can be attributed to clumping and internal friction within the aggregate skeleton [42–44]. The HRWR demand was particularly high at 0.85% PP fibers, reaching 4.04%.

Table 1. Concrete mechanical properties and shear strengths of RC beams.

Mix	HRWR, % of Cem.	Mechanical Properties				Shear Strength Properties			
		$f_c^{'}$, MPa	f_t, MPa	E, GPa,	f_r, MPa	Load for 1st Crack, kN	P_{max}, kN	δ_{max}, mm	Max. Crack Opening, mm
Control	1.67	41.5 (4.8%)	3.2 (5.8%)	29.5 (6.2)	4.41 (5%)	68 (14%)	73.23 (7.6%)	2.74 (10.5%)	0.63 (12.2%)
1% PVA	3.56	41.2 (6.5%)	4.32 (7%)	27.6 (8%)	6.21 (5.8%)	91 (9.5%)	109.87 (9.2%)	3.66 (13.3%)	0.28 (8.8%)
0.5% PP	3.19	33.7 (6%)	2.64 (6.4%)	29.3 (8.3%)	5.05 (6.1%)	73 (11%)	82.02 (7.9%)	3.41 (15%)	0.48 (10.2%)
0.85% PP	4.04	30.7 (7.2%)	2.93 (7.3%)	24.8 (9%)	4.92 (7.4%)	84.5 (16.6%)	101.1 (12.2%)	4.7 (14.2%)	0.33 (9.6%)

COV values are given between parenthesis.

The concrete's compressive strength ($f_c^{'}$), splitting tensile strength (f_t), and modulus of elasticity (E) were determined using 100 × 200-mm cylindrical specimens, as per ASTM C39, C496, and C469, respectively [45–48]. The flexural strength (f_r) was determined using 75 × 75 × 280 mm prisms by third-point bending, as per ASTM C78 (2018). Curing was performed at 95% relative humidity and 23 °C ambient temperature for 28 days. The mean of 5 measurements is reported in Table 1, along with the coefficients of variation (COV), computed as the ratio between the standard deviation for the various measurements divided by the mean value.

As shown in Table 1, the compression-related properties (i.e., $f_c^{'}$ and E) for the PVA fiber mix remained fairly close to the control value and within the repeatability of testing. In contrast, those measurements decreased to 30.7 MPa and 24.8 GPa with 0.85% PP additions. This drop could be related to the high HRWR demand that increased internal bleeding and water accumulation around the PP filaments, thus creating additional porosity and weakening the bonding strength within the cement matrix [49,50]. The f_r responses improved with PVA or PP fibers, which can be attributed to a bridging effect that limits the initiation and propagation of cracks during loading [51,52]. Hence, the control f_r value of 4.41 MPa increased to 4.92 and 5.58 MPa with the addition of 0.85% PP or 1% PVA fibers, respectively.

3.2. Shear Strength Properties of RC Beams

Duplicate RC beams configured without stirrups are tested in this work [41]. The beams, measuring 780-mm long and 150 × 150 mm^2 in cross-section, were mounted on a simply supported set-up and subjected to two-point vertical loading at a rate of 4 kN/min until failure. Figure 1 shows the beam dimensions, distribution of reinforcing bars, application of two-point forces, and LVDT for measuring the mid-span deflection. Two 16-mm diameter longitudinal steel sections are used in the tension zone, while four stirrups are positioned at the supports and under the loading points. The steel's Young's modulus of elasticity (E_s) and yield stress (f_y) are 200 ± 25 GPa and 510 ± 40 MPa, respectively. The concrete is compacted in the beams using a laboratory vibrator, demolded after 24 h and cured for 28 days at 95% relative humidity. Table 1 summarizes the beams' shear strength

properties, including the load at which the first diagonal shear crack appeared, ultimate load (P_{max}), corresponding deflection (δ_{max}), and maximum crack opening at failure.

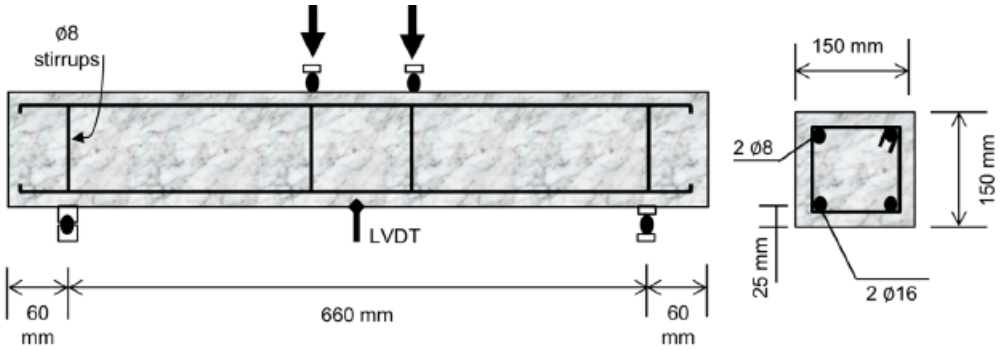


Figure 1. Set-up configuration employed for assessing shear strength of RC beams.

Figure 2 shows the crack patterns observed at failure for the various tested RC beams. The control concrete failed along two diagonal shear cracks and developed a maximum opening of 0.63 mm. The cracks started from the support and propagated upwards at an angle of about 30–40 degrees from the horizontal. When the PVA and PP fibers are introduced, fewer and finer vertical flexural cracks are formed, which may be attributed to the fiber bridging effect that reduced crack formation in the tension zone [41]. The failure of beams containing fibers was more gradual, and occurred along one major shear crack that propagated at about 30 degrees from the horizontal. Hence, the load at which the first diagonal crack appeared increased from 68 kN for the control beam to 91 and 84.5 kN when 1% PVA or 0.85% PP fibers were introduced. The resulting maximum crack openings were 0.28 and 0.33 mm, respectively.

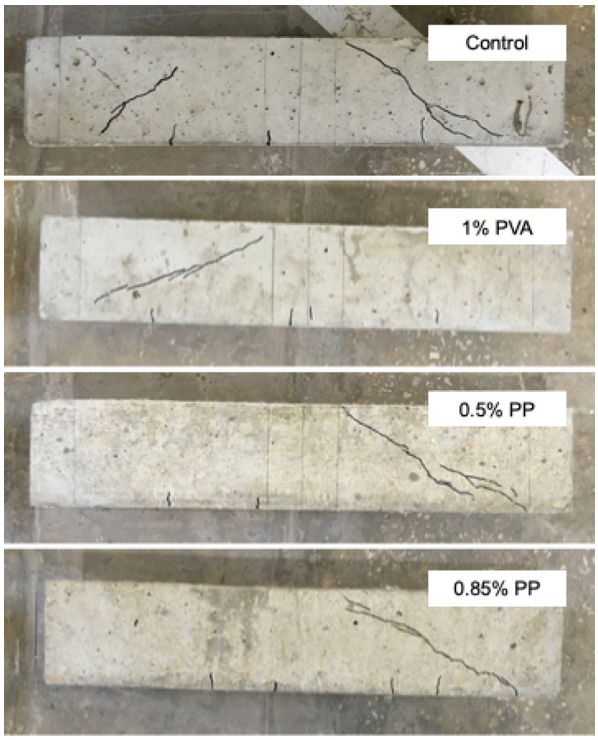


Figure 2. Crack patterns of RC beams with or without PP or PVA fibers.

The incorporation of fibers significantly improved the P_{max} and δ_{max} values (Table 1). For example, the P_{max} of 73.23 kN registered for the control beam increased to 82.02 and 101.1 kN for mixtures containing 0.5% or 0.85% PP fibers, respectively. The corresponding

δ_{max} increased from 2.74 to 3.41 and 4.7 mm, respectively. Earlier studies showed that such improvement could be related to the fiber bridging effect that prevents the cracks from further opening during loading, thus leading to enhanced dowel action of the longitudinal reinforcement and aggregate interlock mechanism along the diagonal fractured surfaces [53–55]. The highest P_{max} of 109.87 kN was achieved with 1% PVA fibers, given the increased chemical and frictional bonds between the PVA filaments and cement matrix.

4. Deterministic FE Model Results

4.1. Description of the Model

The processing FE software used in this study is Cast3m (version 2024) [56], which is commonly employed to minimize computational costs for two-dimensional plane stresses where the out-of-plane effects are considered negligible [56]. As shown in Figure 3, the steel reinforcing bars are represented by one-dimensional bar elements, while the concrete consists of a uniform two-dimensional quadrilateral mesh with 1-mm element size, incorporating bilinear finite elements. Small elastic areas are used to avoid damage in the support points and loading. The end nodes at the bottom of the beam are blocked vertically, while one of them (i.e., right node) is also blocked horizontally. The monitoring points in the described FE model include the nodes at load application and the middle of the bottom face of the beam for the displacement.

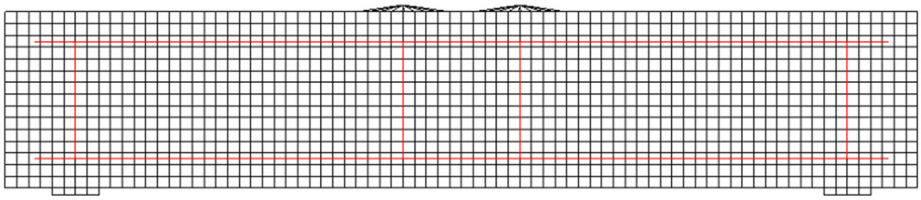


Figure 3. Mesh representation of modeled RC beam (red lines represent the steel bars).

Steel reinforcement is modeled using the elastoplastic method with constant stress after hardening, while a perfect bond is considered between the concrete and steel bars. Figure 4 gives the distribution of tensile stress along the length of the bottom reinforcing bar for the 4 different mixes, at peak load. As shown in the Figure 4, between the inner loading points, the tensile strength remains uniform and less than the yield stress of the bar equal to 520 MPa.

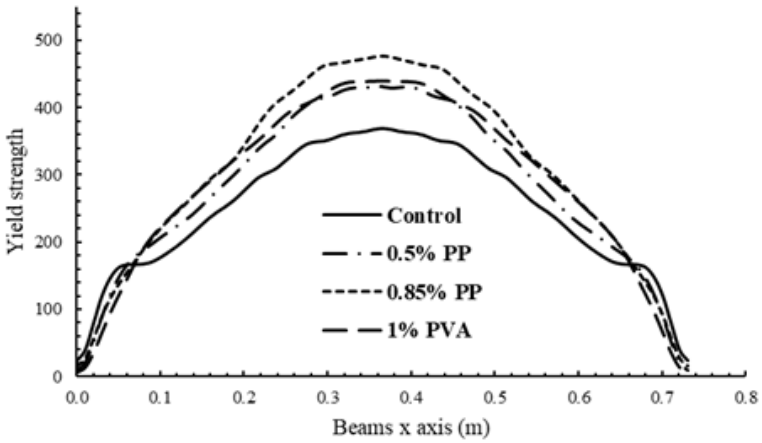


Figure 4. Distribution of yield stress along the bottom longitudinal reinforcement, at failure, for the different FRC mixes.

Mazar's isotropic damage model is used [57], with the progressive concrete degradation described by a scalar damage variable (D). The internal variable establishes a

relationship between the stress tensor (σ) and strain tensor (ε), as expressed in Equation (1).

$$\sigma = (1 - D)E\varepsilon \quad (1)$$

where E denotes the elasticity tensor, while the D variable ranges from 0, representing an undamaged material, to 1, indicating complete failure. According to the model proposed by Mazar [57], D depends on the equivalent strain ($\varepsilon_{eq} = \sqrt{\sum_{i=1}^{3} \varepsilon_i^+}$) during the loading and the damage threshold $\varepsilon_{D0} = f_t/E$. The equivalent strain is taken initially equal to the damage threshold. The damage evolution law states:

$$D = 1 - \frac{\varepsilon_{D0}}{\varepsilon_{eq}}\left(1 - \alpha + \alpha\exp\left(-\beta\left(\varepsilon_{eq} - \varepsilon_{D0}\right)\right)\right) \quad (2)$$

where α and β are parameters of the model.

To address the mesh dependency, the stress-based regularization nonlocal approach is employed [58], which is based on the weighting function given in Equation (3).

$$\varphi(x - s) = \exp\left(-\left(\frac{2||x - s||}{l_c \rho(x, \sigma(s))}\right)^2\right) \quad (3)$$

The internal length (l_c) is selected to constrain the spread of nonlocal damage and ensure accurate damage initiation. This length is set to equal the maximum aggregate size (i.e., 20 mm). The load is applied incrementally at two points on the modelled beam, as in the experimental setup. The loading points are modeled as small triangular areas (2.5 × 12 mm) to mitigate stress concentration, while the supports are modelled as rectangular elastic areas (2.5 × 10 mm) to prevent geometric singularities. The load is applied at increasingly vertical displacement, ranging up to 7 mm, depending on the FRC type, and software is run to determine the crack patterns and load-deflection curves until failure.

4.2. Field Damage Distribution

Figures 5–8 show the distribution of the scalar damage (D) variable at various loading levels of 50%, 75%, and 100% P_{max} for the tested RC beams. These plots represent the crack propagation and opening, providing deeper insight into the crack distribution and progression at different loading stages. The blue areas indicate no damage (D = 0.98), while the red areas (D = 1.00) highlight the damaged regions and crack locations. Figures 5–8 also show the comparison between the experimental and numerical load-deflection curves, which will be discussed later.

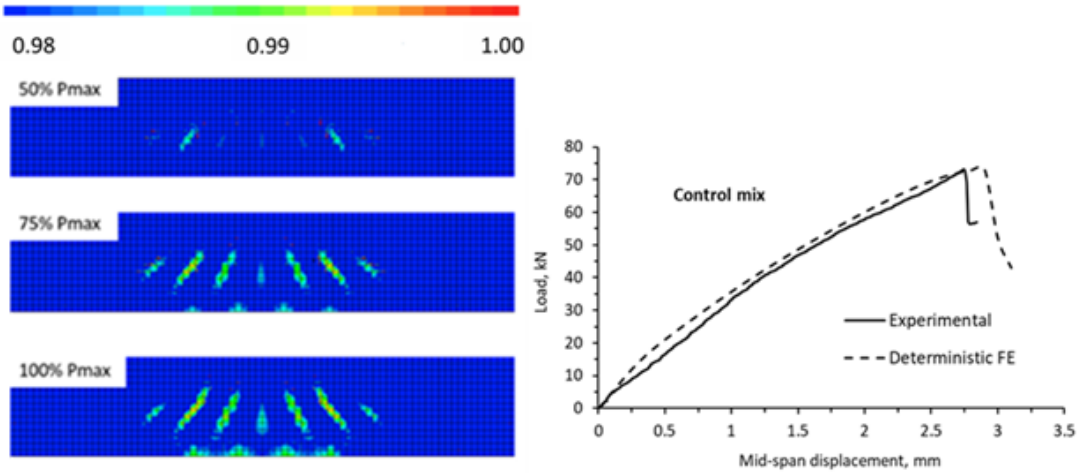


Figure 5. Damage field distribution at different load levels and load-deflection curves for the control beam.

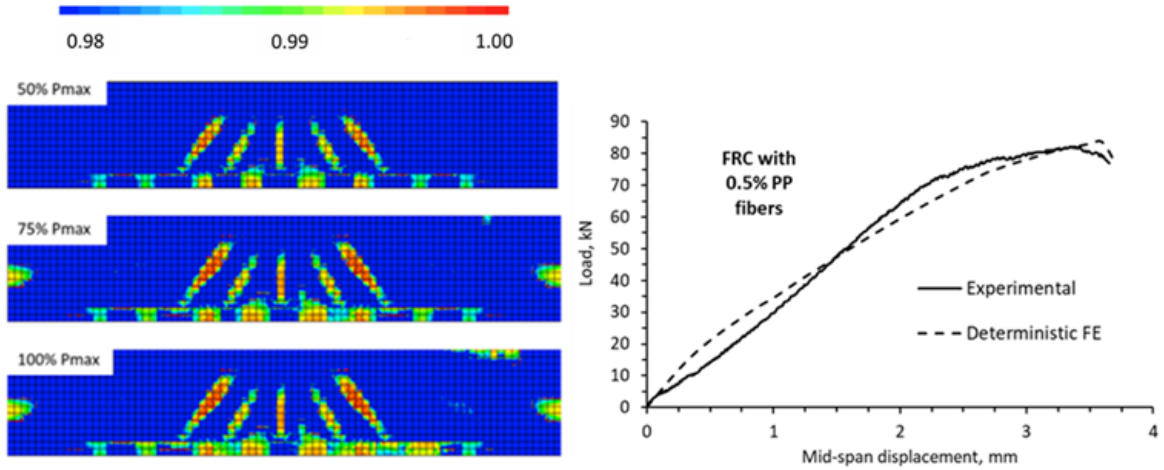


Figure 6. Damage field distribution at different load levels and load-deflection curves for the beam containing 0.5% PP fibers.

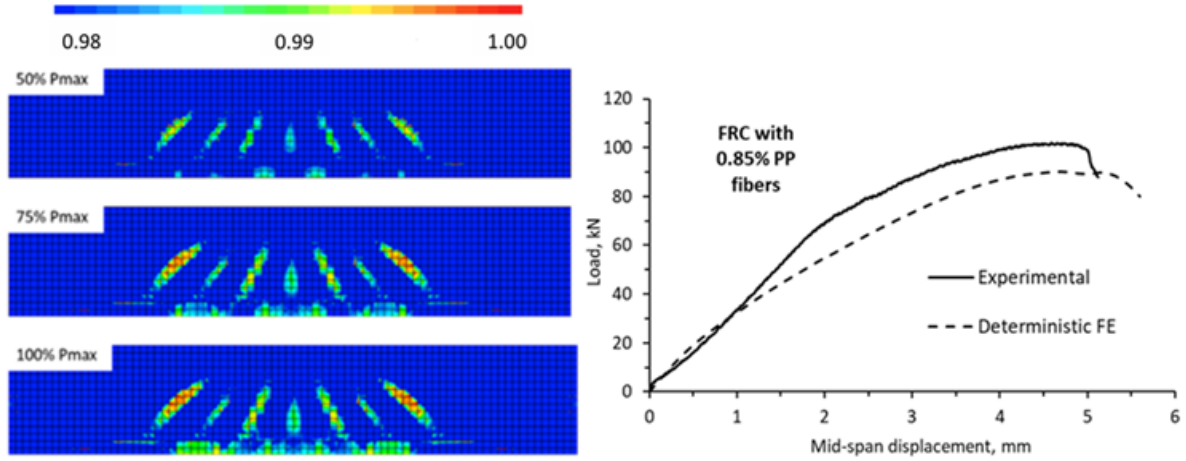


Figure 7. Damage field distribution at different load levels and load-deflection curves for the beam containing 0.85% PP fibers.

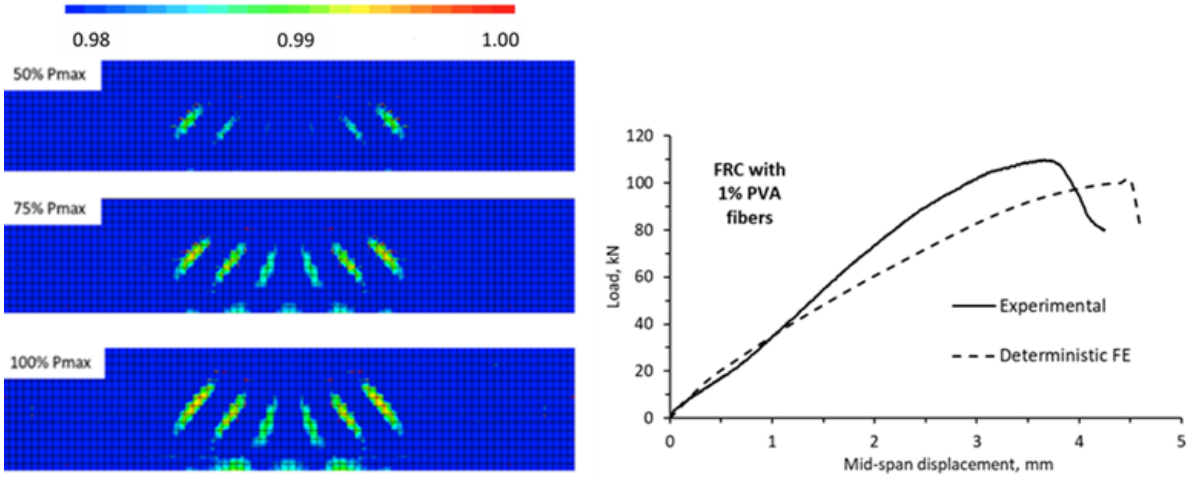


Figure 8. Damage field distribution at different load levels and load-deflection curves for the beam containing 1% PVA fibers.

As shown in the damage field distribution plots, the deterministic model showed limited numbers of diagonal cracks at 50% P_{max} for the beam prepared with fiber-free concrete (Figure 4), while these were more visible when the FRC beams were used (Figures 6–8).

This could be associated with the reduced modulus of elasticity; the E value dropped from 29.5 GPa for the control concrete to 27.6 and 24.8 GPa for FRC containing 1% PVA or 0.85% PP fibers, respectively. The increased deformation at a given load is expected to transmit tensile stresses throughout the concrete, causing the release of energy to other locations, leading to the formation of more cracks [55].

Regardless of the concrete type, the damaged areas that were computed numerically become evident at 75% P_{max} and were found to develop along two symmetrical cracks formed at 45 degree angles from the horizontal axis (Figures 5–8). The cracks propagated gradually as the load increased towards the shear span regions, and became wider and deeper until failure. This behavior, however, was distinctly different from the experimental testing in two respects, including the relative load at which the first cracks appeared and the number of cracks at failure. The diagonal cracks were invisible at 75% P_{max} during experimental testing, as summarized in Table 1, and the first crack appeared at 93% P_{max} for the control beam and varied between 84% to 89% P_{max} for the FRC beams. This confirms the relevance of FE modeling to forecast the initiation of cracks and damaged areas during the different loading stages. On the other hand, only the control beam exhibited two diagonal cracks at failure during the experimental testing (Figure 2), while the remaining FRC beams showed only one crack. This differs from the results of the FE model, which yielded two symmetrical cracks in all cases, given the basic deterministic principle that states the mechanical properties of concrete are constant throughout the structural members. As will be discussed later, this highlights the utility of the stochastic FE approach, which treats the concrete, in particular FRC, as heterogenous material, in order to better represent the cracking patterns.

4.3. The Load-Deflection Curves

Regardless of fiber type, the numerical and experimental load-deflection curves were reasonably close to each other (Figures 5–8). The load increased linearly at the initial stages, until reaching the peak value (i.e., P_{max}) indicating the beam's failure. Hence, the P_{max} as computed numerically increased from 72.45 kN for the control beam to 83.51 and 90.38 kN for beams containing 0.5% or 0.85% PP fibers, respectively, while this reached 101.08 kN for the beam made with 1% PVA fiber. Compared to the experimental results summarized in Table 1, the relative error in estimating P_{max} was 1.06% for the control beam, but increased remarkably, to 8% and 10.9%, for the beams containing 1% PVA or 0.85% PP fibers, respectively. As earlier noted, this can be attributed to the deterministic FE approach, which under-estimates the variability of the FRC mechanical properties as a result of the fibers' spatial distribution and clumping tendency within the mass structure.

The maximum mid-span deflection (δ_{max}) recorded numerically for the control beam and beams containing PP fibers were very close to the experimental values (Table 1). Hence, the numerical δ_{max} varied from 2.77 mm for the control beam to 3.6 and 4.76 mm for the beams containing 0.5% or 0.85% PP fibers, respectively. The corresponding relative errors were 0.7%, 5.5%, and 1.27%, respectively. Nevertheless, the FE model over-estimated the deflection for the beam containing 1% PVA fibers, reaching a computed value of 4.5 mm (i.e., 22.9% deviation from the experimental value). This overestimation is due to the Mazar's model, which depends on the FRC's mechanical properties (i.e., f'_c, f_t, and E), including the strain level at which the micro-damage begins to accumulate due to the presence of fibers [52–54]. Figure 9 plots the relationships between P_{max} and δ_{max}; as shown, the correlation coefficient (R^2) improved from 0.5 (dotted line) to 0.77 (continuous line) when the values were determined numerically.

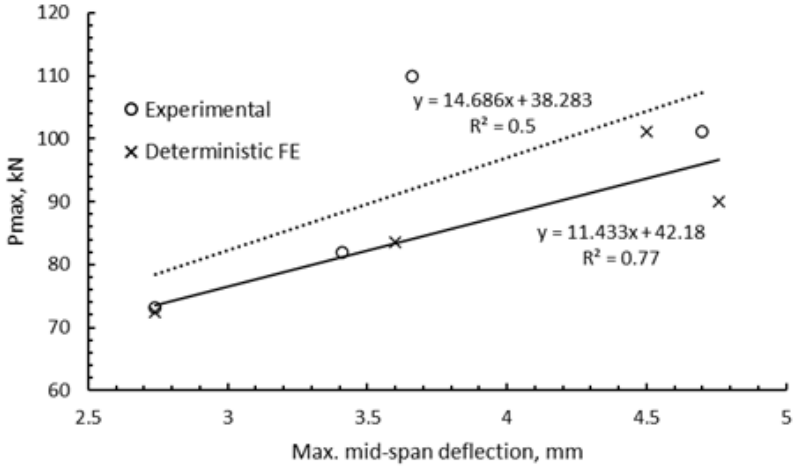


Figure 9. Relationships between P_{max} and δ_{max} determined experimentally or numerically.

5. Stochastic FE Model Results

The heterogeneity of concrete increases with the addition of fibers, as reflected by the higher spatial variability of the mechanical properties. For example, the COV for f_t and E increased by 25.8% and 45.1%, respectively, for the FRC containing 0.85% PP fibers compared to the control mix (Table 1). Hence, this section discusses the suitability of the stochastic FE approach to assess the effect of spatial FRC variability on cracking behavior and damage thresholds, using the following two approaches:

- Random fields (RF), involving the discretized random values at different locations of the considered spatial domain, guided by the specified statistical properties and autocorrelation input (i.e., functions and lengths). The effect of the uncertainty on the quantities of interest (i.e., critical stress, threshold displacement, probability of failure, etc.) is assessed by means of an adequate uncertainty propagation method, such as the well-known Monte Carlo simulation [38,59–61].
- Random variables (RV), considering the RC beam as a homogeneous member within a single simulation. The spatial variability is then generated by mean of various different samples, according to the respective distributions and statistical characteristics of the uncertain parameter [36,37,62].

5.1. Uncertainties of Stochastic Modeling Based on RF Generation

5.1.1. Description of the RF Approach

The RF approach is characterized by a mean function (μ (**z**)), covariance function (C_{vv} (**z**, **z**′)), autocorrelation function (ρ (**z**, **z**′)) to describe the statistical dependency between two points of the spatial domain, and standard deviation (σ), which measures the difference from the mean value. The C_{vv} (**z**, **z**′) and ρ (**z**, **z**′) can be written in Equations (4) and (5) as:

$$C_{vv}(\mathbf{z}, \mathbf{z}') = \sigma(\mathbf{z})\sigma(\mathbf{z}')\rho(\mathbf{z}, \mathbf{z}') \quad (4)$$

$$\rho(\mathbf{z}, \mathbf{z}') = \exp\left(-\left(\frac{\mathbf{z} - \mathbf{z}'}{a}\right)^2\right) \quad (5)$$

The Gaussian autocorrelation function depends on the relative distance between two points, **z** and **z′**, which called the autocorrelation length a [34]. A greater autocorrelation length indicates a stronger correlation between the various points in the same field. In order to accurately model the spatial variability of concrete properties, a is taken as equal to the concrete maximum aggregate size, which is 20 mm.

The Choleski decomposition is selected to generate realizations of RF [59,61]. This approach expresses the random vector $\widetilde{V}_G$ as the sum of the expected mean value of the random field and a linear combination of standard Gaussian random variables Y ($Y = \{Y_k, k = 1 \ldots n_G\}$), which have zero mean and unit variance. The formulation is given by $\widetilde{V}_G(\mathbf{z}) = \mu + BY$, where B is a square matrix satisfying $C_{ij} = BB^T$. The discretized RF defined on the two-dimensional mesh is then projected in the FE mesh given in Equation (6), where n_{FE} denotes the number of nodes in the FE mesh.

$$\widetilde{V}_G(\mathbf{z}) = \{V_{Gk}, k = 1 \ldots n_G\} \rightarrow \widetilde{V}_{FE}(x) = \{V_{FEk}, k = 1 \ldots n_{FE}\} \quad (6)$$

The RF are generated using either f_t or E responses, given their significant effect on the damage patterns and failure modes [63,64]. For example, for a beam containing 0.85% PP fibers, two RF are generated, i.e., one using E responses, having a mean value of 24.8 GPa and standard deviation of 2.23 GPa, and another using f_t, having a mean of 2.93 MPa and standard deviation of 0.21 MPa. Their spatial variability is described by means of a discretized random field defined on a two-dimensional grid consisting of n_G nodes, as expressed in Equation (7):

$$V(\mathbf{z}) \rightarrow \widetilde{V}_G(\mathbf{z}) = \{V_{Gk}, k = 1 \ldots n_G\} \quad (7)$$

The discretization method involves approximating the original random field $V(\mathbf{z})$ with a finite set of random variables that are assembled into a random vector $\widetilde{V}_G$. For each f_t or E response, a sufficient number of RF iterations (i.e., 30 iterations) are realized to ensure a balance between the efficiency of computation and the accuracy and statistical characteristics for the uncertain parameters [63]. The uncertainty propagation on P_{max}, δ_{max}, and cracking patterns are studied, as discussed below.

5.1.2. Prediction of Load-Deflection Curves Through RF Generation

Figure 10 compares the experimental and numerical load-deflection curves for the control beam and beams containing 0.5% PP, 0.85% PP, and 1% PVA fibers. The numerical curves correspond to the lower and upper P_{max} values that resulted from the various RF realizations using either f_t or E responses. Clearly, all of the curves yielded the same behavior, characterized by a linear load at the initial stages until reaching P_{max}, indicating the beam's failure. Nevertheless, unlike the deterministic FE approach, the variability in the mechanical properties (i.e., f_t or E) introduced a range of peak loads and deflections, reflecting the benefits of the stochastic RF modeling to predict the range of failure boundaries, along with their conservative values for the safe design and evaluation of FRC beams. In fact, the scattering in mechanical properties amplifies the differences in the pre- or post-peak behaviors across realizations, with some exhibiting sudden drops and others showing more gradual declines.

A sensitivity analysis conducted on the plots shown in Figure 10 shows that the E parameter is better than f_t for determining the uncertainty of P_{max} and δ_{max} propagations due to fiber additions. For example, in the case of the beam containing 0.85% PP fibers, the experimental P_{max} of 101.1 kN lies within the lower and upper values (i.e., 88.5 and 103.9 kN, respectively) when E is considered. On the other hand, when the scattering of f_t is considered, the experimental P_{max} falls outside the envelope, with a lower value of 85.1 kN and upper value of 97.1 kN. In other words, the variation of f_t leads to deterministic elastic behavior and a random post-peak, whereas the variation of E affects both the pre- and post-peak behaviors. It can thus be concluded that the spatial randomness of E is associated with a better cumulative distribution function on P_{max} and δ_{max}, allowing a more realistic assessment of the FRC beam performance. Recall that PP and PVA fibers

generally have a negligible effect on the E due to their low stiffness compared to the cement matrix. However, they significantly enhance f_t, as PVA fibers exhibit strong bonding with the matrix, improving crack resistance, while PP fibers enhance ductility and energy absorption, reducing crack propagation. The heterogeneities in FRC mixtures are more influenced by the spatial scattering of E.

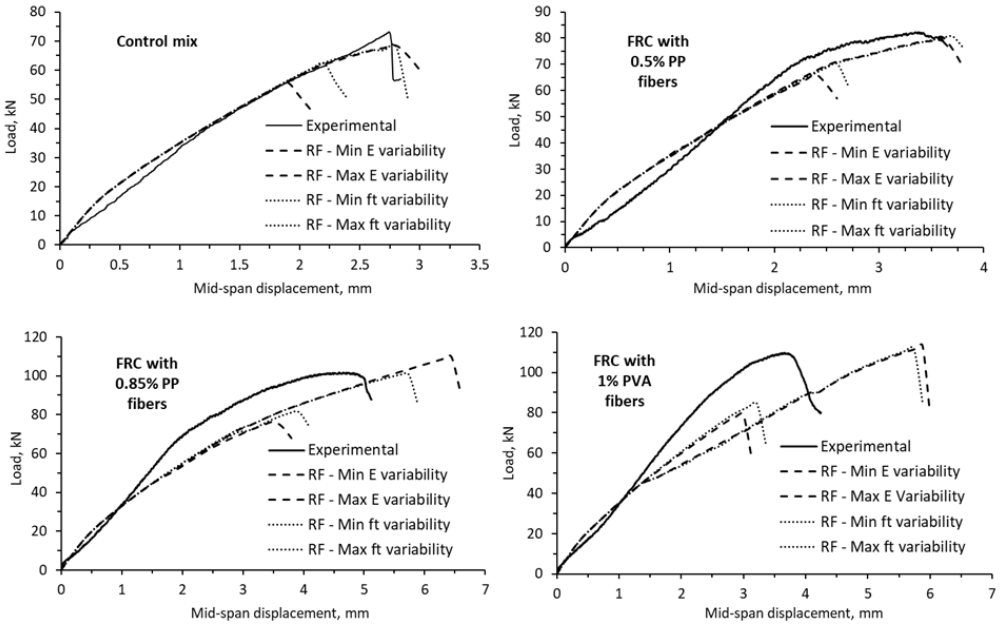


Figure 10. Load-deflection curves for all beams obtained experimentally and numerically, using the RF approach with f_t and E variability.

5.1.3. Prediction of Cracking Patterns Through RF Generation

Figures 11–13 represent typical random field (RF) realizations and corresponding equivalent strain (ε_{eq}) distributions obtained at failure for the control beam and beams containing 0.85% PP and 1% PVA fibers. The plots are created using varying E and f_t responses, and correspond to the upper and lower load-deflection curves. In most of the RF realizations, the control fiber-free beam exhibtied two major symmetrical diagonal shear cracks at failure (i.e., similar to the deterministic model), suggesting that the spatial variability introduced in those realizations is insufficient, which causes the cracks to propagate in a similar pattern. The concrete is thus treated as a homogeneous material, which results in mirroring of the tensile stress distribution on both sides of the beam. This cracking pattern accords fairly well with the two major diagonal shear cracks observed in the experimental tests for the control beam (Figure 2). On the other hand, the FRC beams containing PP or PVA fibers exhibited a substantially different cracking pattern, characterized by a single crack, either on the left or right side of the beam (Figures 12 and 13). In these cases, the spatial scattering leads to random localization and propagation of cracks in the FE model. This type of single crack formation resembles the patterns observed during experimental testing of the FRC beams (Figure 2).

As shown in Figures 11–13 and Table 2, the maximum ε_{eq} for the tested beams seems to be higher when considering the spatial variability of E, reaching 9×10^{-2} for the FRC containing 1% PVA fibers. This confirms that E influences strain accumulation and redistribution, which in turn affects the cracking patterns and damage progression in the material. In addition, the ε_{eq} increases when fibers are added to the concrete, especially when considering the variability E (instead of f_t). This reflects the impact of E on strain accumulation and redistribution, leading to a reduced number of flexural cracks being formed due to the bridging effect and reduction of cracks in the tension zone [38]. Hence,

managing the variability of E is essential for shaping the load-deflection behavior and understanding the structural performance of FRC beams.

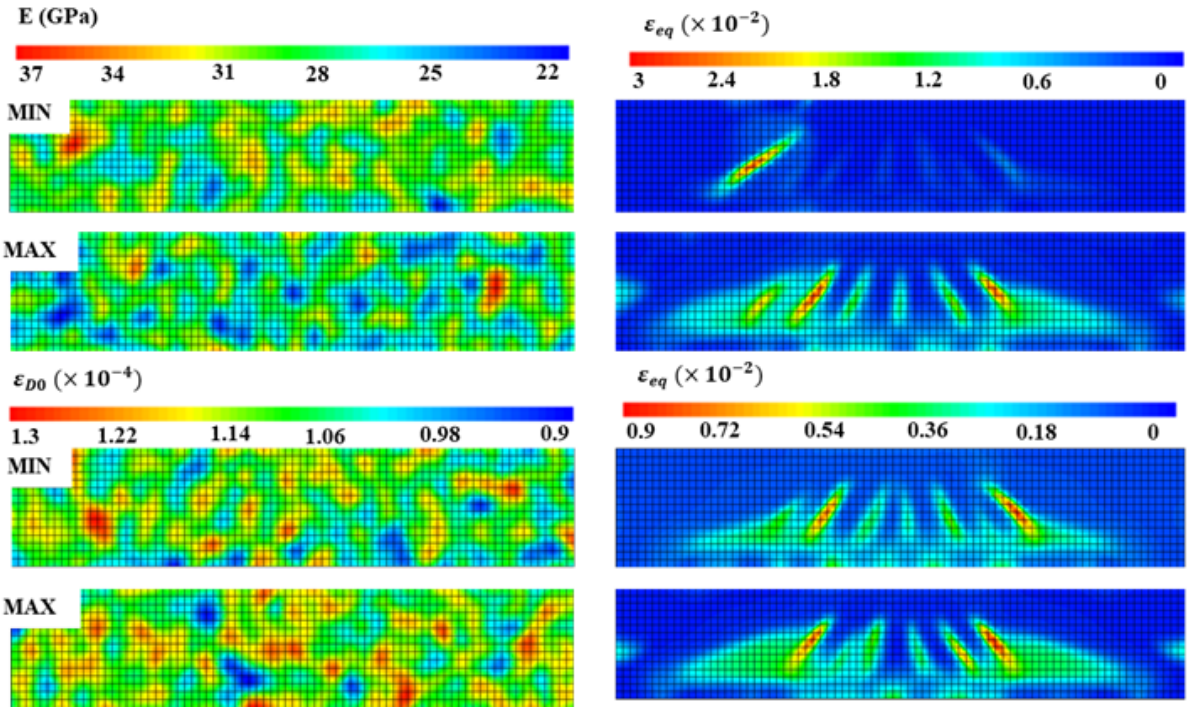


Figure 11. Random field realizations of E and f_t for the control beam at the lower and upper load-deflection curves and their corresponding ε_{eq} distributions at failure.

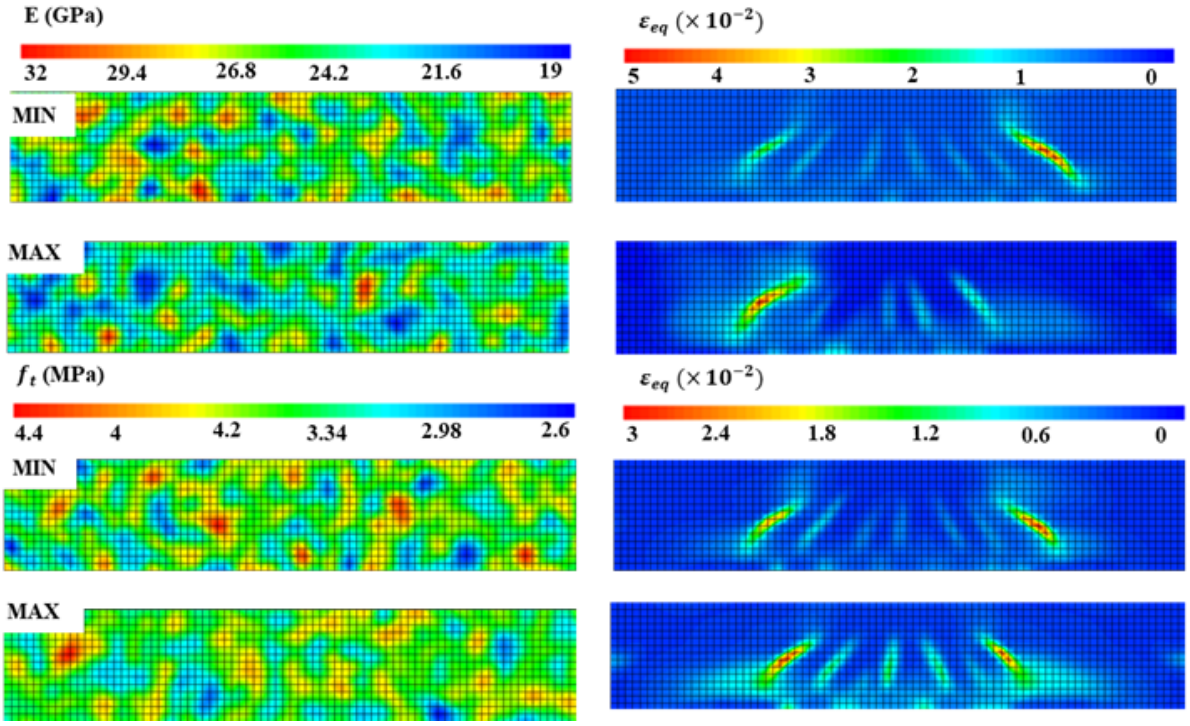


Figure 12. Random field realizations of E and f_t for the 0.85% PP fiber beam at the lower and upper load-deflection curves and their corresponding ε_{eq} distributions at failure.

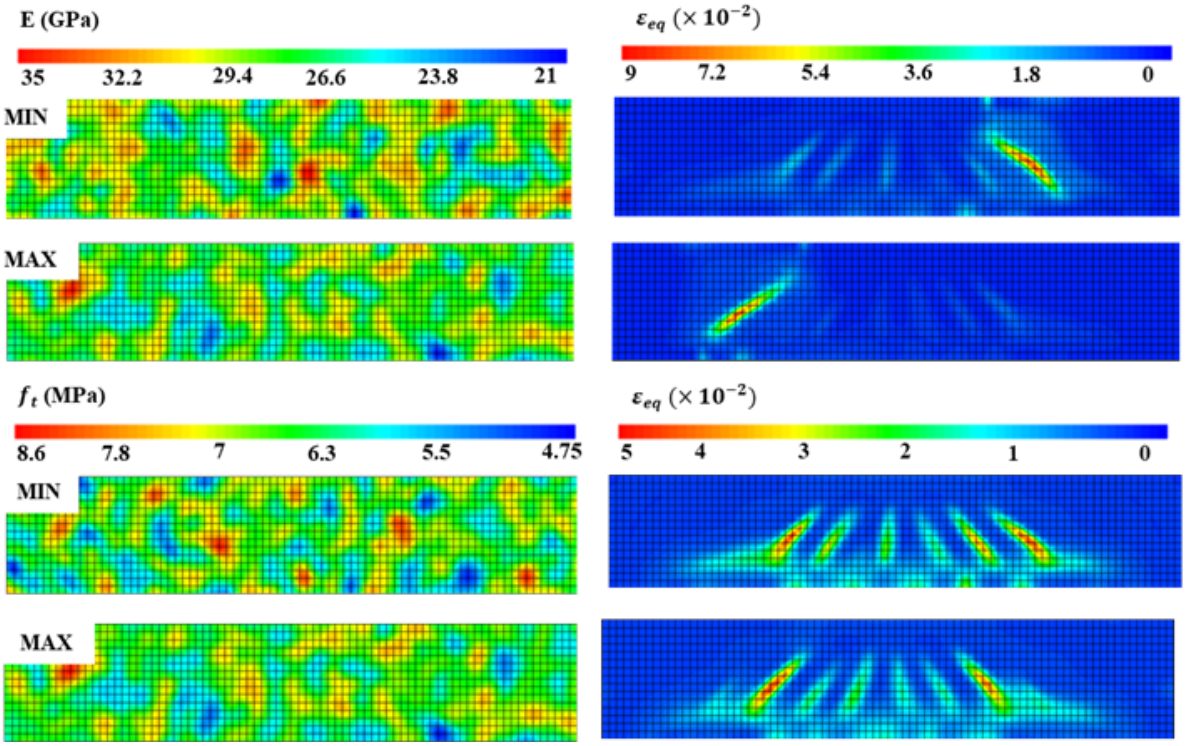


Figure 13. Random field realizations of E and f_t for 1% PVA fiber beam at the lower and upper load-deflection curves and their corresponding ε_{eq} distributions at failure.

Table 2. Maximum values of ε_{eq}, obtained at failure, for the different FRC mixtures, using variability f_t and variability E.

	Control	0.5% PP	0.85% PP	1% PVA
Variability f_t	0.9×10^{-2}	1.5×10^{-2}	3×10^{-2}	5×10^{-2}
Variability E	3×10^{-2}	3.8×10^{-2}	5×10^{-2}	9×10^{-2}

Depending on whether the generated realization and distribution of weak points are represented by f_t or E, cracking patterns with a single major crack will differ in their statistical influence. The cracking of concrete is showed to be influenced by the heterogeneity introduced through RF, where some realizations create weak zones at a certain region and initiate the formation of a single crack. Based on 30 generated realizations of the defined random field, the frequencies of each cracking pattern appear to be strongly dependent on the choice of random property. As shown in Figure 14, when E is used, the frequency of a cracking pattern with a single major crack is significantly higher than that of two diagonal cracks in FRC beams, reaching nearly 70%. For instance, in the case of the beam containing 0.85% PP fibers, the probability of forming a single dominant crack is 70% with variability in E, compared to 37.9% with variability in f_t. Thus, the cracking behavior of PP and PVA fiber beams is mostly influenced by the variability of E, which maximizes the statistical effect on the cracking pattern.

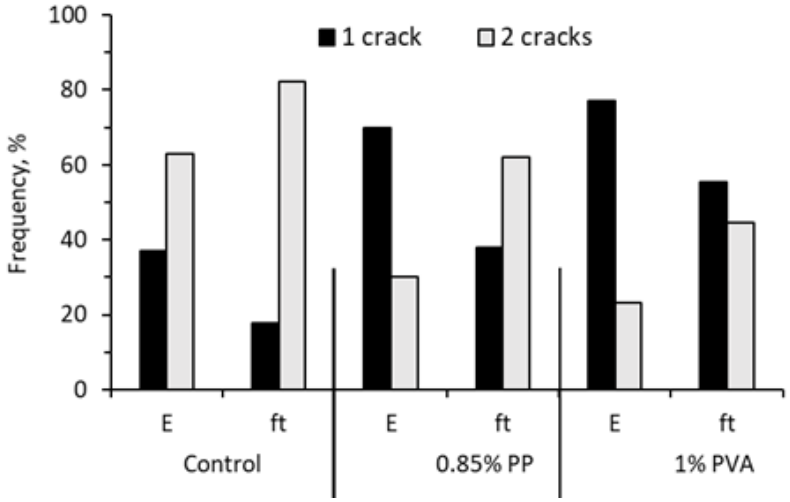


Figure 14. Frequency of cracking pattern distribution as function of E or f_t.

5.2. Uncertainties of Stochastic Modeling Based on RV Generation

Monte Carlo simulations by random variable (RV) generation are performed for each beam, considering the Young's modulus as an uncertain parameter, since this has previously been found to significant impact the load-deflection curves and cracking patterns of beams. The simulations involved 50 runs of the FE model, where the uncertain E parameter is sampled according to a Gaussian distribution, with the mean and standard deviation corresponding to the values reported in Table 1. Figure 15 displays the simulation convergence for the estimated mean and standard deviation of P_{max}. As can be seen, good convergence achieved, as the statistical moments of interest no longer vary after 50 runs of the FE model.

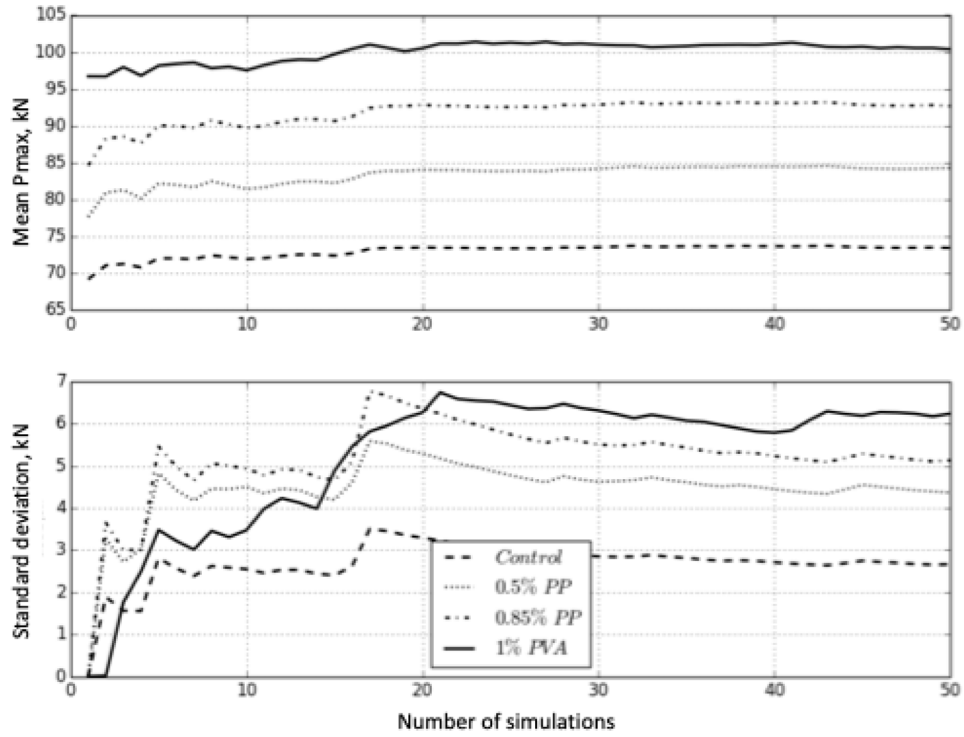


Figure 15. Convergence of Monte Carlo simulations based on RV generation.

Table 3 compares the mean P_{max} and δ_{max} values determined experimentally to those computed numerically, along with the resulting deviation and COV. As shown, the mean values of P_{max} and δ_{max} are accurately predicted using RV generation, although with

reduced variability. For example, the experimental-to-numerical P_{max} for the control beam was 73.23-to-73.51 kN for the control beam, and 82.02-to-84.23 kN for the beam containing 0.5% PP fibers. However, the corresponding experimental-to-numerical COV dropped remarkably, to 7.6-to-3.6% and 7.9-to-3.21%, respectively. The RV method underestimates the scattering of the output parameters, especially when higher percentages of PP and PVA fibers are introduced into the FRC beam. On the other hand, the RF generation seems to be more accurate in estimating the variability of P_{max} and δ_{max}, thus providing closer COV estimates to those derived from the experimental results. The resulting numerical COVs are reasonably close to those determined experimentally, reflecting the relevance of considering the RF spatial variability when evaluating heterogenous materials.

Table 3. Values of P_{max} and δ_{max} obtained experimentally vs. those computed using the RF and RV methods.

	Experimental P_{max}		P_{max} by RF		P_{max} by RV	
	Mean, kN	Deviation, kN COV, %	Mean, kN	Deviation, kN COV, %	Mean, kN	Deviation, kN COV, %
Control	73.23	5.56 (7.6%)	68.19	5.07 (7.44%)	73.51	2.65 (3.6%)
0.5% PP	82.02	6.48 (7.9%)	76.41	5.7 (7.46%)	84.23	4.39 (3.21%)
0.85% PP	101.1	12.33 (12.2%)	95.29	8.57 (9%)	92.67	5.12 (5.53%)
1% PVA	109.87	10.11 (9.2%)	94.6	9.21 (9.74%)	100.37	6.24 (6.22%)
	Experimental δ_{max}		δ_{max} by RF		δ_{max} by RV	
	Mean, mm	Deviation, mm COV, %	Mean, mm	Deviation, mm COV, %	Mean, mm	Deviation, mm COV, %
Control	2.74	0.28 (10.5%)	2.69	0.43 (15.9%)	2.9	0.013 (0.5%)
0.5% PP	3.41	0.51 (15%)	3.24	0.55 (17%)	3.6	0.028 (0.77%)
0.85% PP	4.7	0.67 (14.2%)	5.28	0.71 (13.5%)	4.32	0.07 (1.6%)
1% PVA	3.66	0.48 (13.3%)	4.34	0.9 (20.8%)	4.23	0.03 (1.7%)

Figure 16 plots the relationships between E with respect to P_{max} and δ_{max}, determined experimentally or numerically using RV and RF generations. As shown, the R^2 increased from 0.5 for the experimental data to 0.64 using RF generation, while the data generated from RV yielded the lowest R^2 of 0.39. This also applies for the relationship between E and δ_{max}, where the highest R^2 of 0.91 resulted from the RF generation. This reflects the importance of considering the RF spatial variability of the Young's modulus to accurately predict the shear strength of FRC beams without stirrups.

Since the stochastic modeling using RF generation proved to be accurate in predicting the scattering of P_{max} and δ_{max} values, Figure 17 illustrates the cumulative density function (CDF) frequency curves based on 30 generated realizations for each tested RC beam. The findings reveal that the FRC containing high fiber contents (i.e., 0.85% PP and 1% PVA) exhibited wider CDF curves, reflecting increased variability in the output parameters. This variability arises from the random distribution of PP and PVA fibers in the concrete, leading to greater fluctuations in the RC beam. The CDF curves are useful for structural engineers, as they provide powerful statistical tools for assessing the behavior and safety of heterogeneous structures, such as FRC beams.

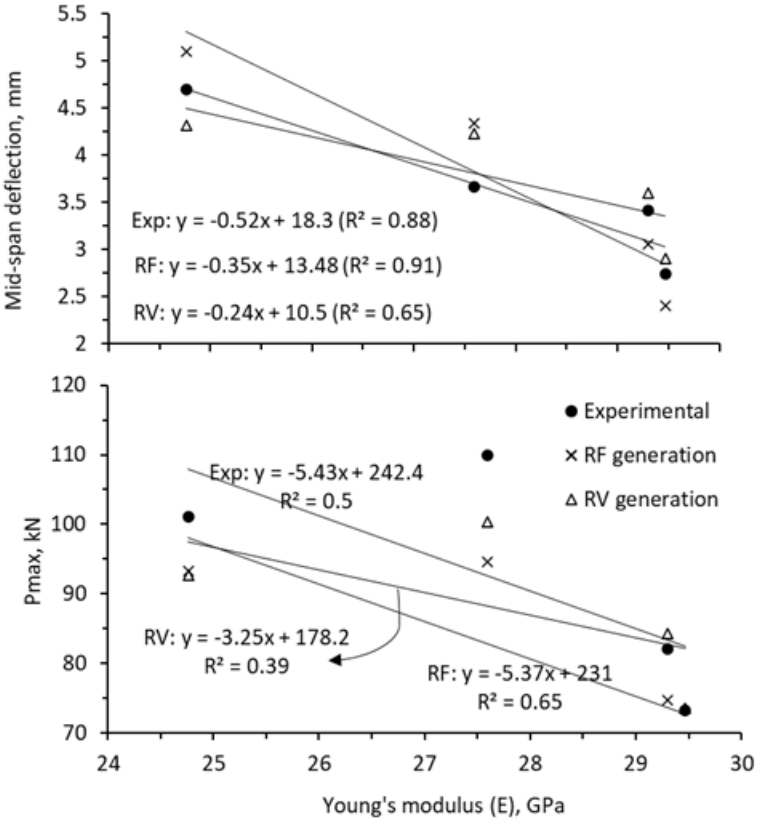


Figure 16. Relationships between the Young's modulus with respect to P_{max} and δ_{max} based on experimental and numerical results.

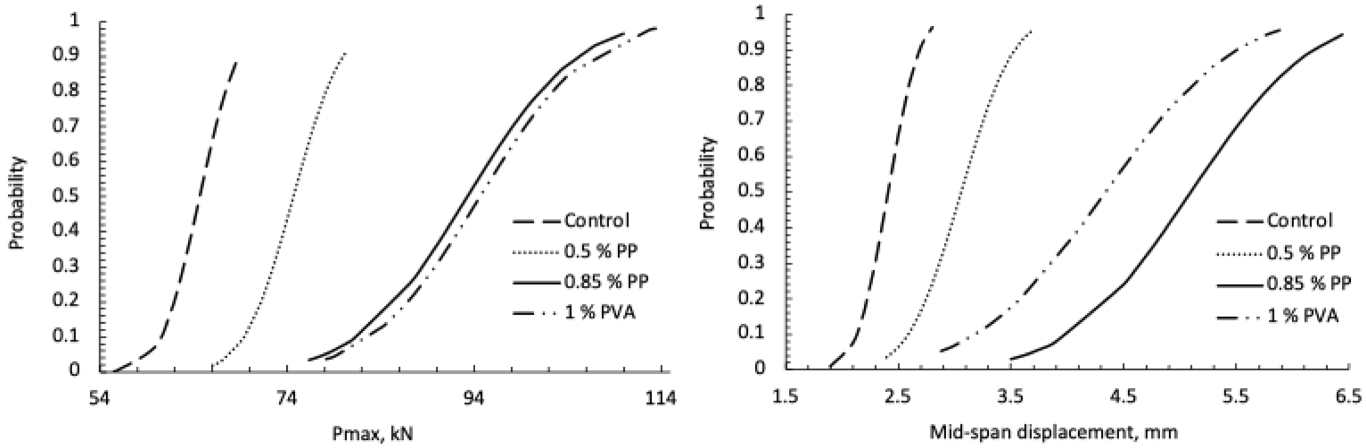


Figure 17. CDF curves for P_{max} and δ_{max} of the tested beams.

6. Conclusions

This paper is part of a comprehensive project undertaken to evaluate the performance of RC beams without stirrups, cast using PP and PVA fiber concrete mixtures. The sensitivity of the structural cracking and ultimate responses to the spatial correlation of concrete damage have been evaluated. Both deterministic and stochastic approaches (based on RF or RV generation) are investigated. The following conclusions have been reached:

- The deterministic FE approach successfully measured P_{max} and δ_{max} with a maximum error of 10.9% and 22.9%, respectively. However, symmetrical damage and crack propagation were noted at the different loading stages, unlike the observed patterns that resulted from experimental testing.

- Unlike the deterministic modelling, the stochastic FE with RF generation yielded a range of P_{max} and δ_{max} values, suggesting the benefits of this approach to predict the range of failure boundaries, in addition to their conservative values for the safe design and evaluation of FRC beams.
- The sensitivity analysis showed that the E parameter is more appropriate than f_t to determine the uncertainty of P_{max} and δ_{max} propagations, due to fiber additions. The spatial randomness of E associated with better strain accumulation and redistribution in FRC beams, which led to fewer flexural cracks in the tension zone.
- The RF generation approximated fairly well the damage and corresponding ε_{eq} distributions at failure. Hence, while the control beam exhibited two major symmetrical diagonal shear cracks at failure, the FRC beams containing PP or PVA fibers showed substantially different cracking patterns, characterized by a single crack, which was identical to the results of experimental testing.
- The P_{max} and δ_{max} values are accurately predicted using stochastic FE with RV generation, although with reduced variability. This is because this method underestimates the scattering of the output parameters, especially when higher percentages of PP and PVA fibers are introduced into the FRC beam. Conversely, RF generation seems to be more accurate in estimating the variability of P_{max} and δ_{max}, and provides closer COV estimates to those derived from experimental results.
- The cumulative density function frequency curves become significantly wider for FRC beams containing high fiber content (i.e., 0.85% PP and 1% PVA), reflecting increased variability in the output parameters. This variability arises from the random distribution of PP and PVA fibers in the concrete, leading to higher performance fluctuations in the RC beam.
- The effectiveness of using SFE with RF generation for FRC beams is validated. However, the discussion primarily focuses on the mechanical property to be modelled as RF. However, RF generation also depends on factors such as the autocorrelation function and autocorrelation length, which have been explored in the literature for plain concrete. Additionally, future research should address the validity of SFE models in predicting the behavior of full-scale beams and the performance of beams with stirrups, designed to fail in flexural mode.

Author Contributions: Software, M.G.; Validation, L.S. and J.K.; Formal analysis, D.N.; Investigation, H.R.; Resources, J.J.A.; Writing—original draft, M.G.; Writing—review & editing, J.J.A.; Project administration, J.K. All authors have read and agreed to the published version of the manuscript.

Funding: This research received no external funding.

Data Availability Statement: The data presented in this study are available on request from the corresponding author on reasonable request.

Conflicts of Interest: The authors declare no conflict of interest.

References

1. Mohammadi, Y.; Singh, S.P.; Kaushik, S.K. Properties of steel fibrous concrete containing mixed fibers in fresh and hardened state. *Constr. Build. Mater.* **2008**, *22*, 956–965. [CrossRef]
2. Shah, A.A.; Ribakov, Y. Recent trends in steel fibered high-strength concrete. *Mater. Des.* **2011**, *32*, 4122–4151. [CrossRef]
3. *ASTM C1116/C1116M—10a*; Standard specification for Fiber-reinforced concrete. ASTM International: West Conshohocken, PA, USA, 2023. [CrossRef]
4. Beglarigale, A.; Yazıcı, H. Pull-out behavior of steel fiber embedded in flowable RPC and ordinary mortar. *Constr. Build. Mater.* **2015**, *75*, 255–265. [CrossRef]
5. Bentur, A.; Mindess, S. *Fibre Reinforced Cementitious Composites*; CRC Press: Boca Raton, FL, USA, 2006.

6. Liu, Y.; Wang, L.; Cao, K.; Sun, L. Review on the Durability of Polypropylene Fibre-Reinforced Concrete. *Adv. Civ. Eng.* **2021**, *2021*, 6652077. [CrossRef]
7. Ramezanianpour, A.; Esmaeili, M.; Ghahari, S.; Najafi, M. Laboratory study on the effect of polypropylene fiber on durability, and physical and mechanical characteristic of concrete for application in sleepers. *Constr. Build. Mater.* **2013**, *44*, 411–418. [CrossRef]
8. Rashid, M.A.; Mansur, M.A. Reinforced High-Strength Concrete Beams in Flexure. *ACI Struct. J.* **2005**, *102*, 462–471.
9. Söylev, T.; Özturan, T. Durability, physical and mechanical properties of fiber-reinforced concretes at low-volume fraction. *Constr. Build. Mater.* **2014**, *73*, 67–75. [CrossRef]
10. Banthia, N.; Gupta, R. Influence of polypropylene fiber geometry on plastic shrinkage cracking in concrete. *Cem. Concr. Res.* **2006**, *36*, 1263–1267. [CrossRef]
11. Khoury, G.A. Concrete spalling assessment methodologies and polypropylene fibre toxicity analysis in tunnel fires. *Struct. Concr.* **2008**, *9*, 11–18. [CrossRef]
12. Matar, P.; Assaad, J.J. Concurrent effects of recycled aggregates and polypropylene fibers on workability and key strength properties of self-consolidating concrete. *Constr. Build. Mater.* **2019**, *199*, 492–500. [CrossRef]
13. Li, V.C.; Wang, S.; Wu, C. Tensile strain-hardening behavior of polyvinyl alcohol engineered cementitious composite (PVA-ECC). *Mater. J.* **2001**, *98*, 483–492.
14. Meng, D.; Lee, C.; Zhang, Y. Flexural and shear behaviours of plain and reinforced polyvinyl alcohol-engineered cementitious composite beams. *Eng. Struct.* **2017**, *151*, 261–272. [CrossRef]
15. Said, S.H.; Razak, H.A. Structural behavior of RC engineered cementitious composite (ECC) exterior beam–column joints under reversed cyclic loading. *Constr. Build. Mater.* **2016**, *107*, 226–234. [CrossRef]
16. Pakravan, H.R.; Ozbakkaloglu, T. Synthetic fibers for cementitious composites: A critical and in-depth review of recent advances. *Constr. Build. Mater.* **2019**, *207*, 491–518. [CrossRef]
17. Yuan, F.; Pan, J.; Xu, Z.; Leung, C.K.Y. A comparison of engineered cementitious composites versus normal concrete in beam-column joints under reversed cyclic loading. *Mater. Struct.* **2013**, *46*, 145–159. [CrossRef]
18. Zhang, P.; Sun, X.; Wei, J.; Wang, J.; Gao, Z. Influence of PVA fibers on the durability of cementitious composites under the wet–heat–salt coupling environment. *Rev. Adv. Mater. Sci.* **2023**, *62*, 20230155. [CrossRef]
19. Abou El-Mal HS, S.; Sherbini, A.S.; Sallam HE, M. Mode II fracture toughness of hybrid FRCs. *Int. J. Concr. Struct. Mater.* **2015**, *9*, 475–486. [CrossRef]
20. Chowdhury, A.; Islam, M.; Zahid, Z.I. Finite Element Modeling of Compressive and Splitting Tensile Behavior of Plain Concrete and Steel Fiber Reinforced Concrete Cylinder Specimens. *Adv. Civ. Eng.* **2016**, *2016*, 6579434. [CrossRef]
21. Guenet, T. Modélisation du comportement des bétons fibrés à ultra-hautes performances par la micromécanique: Effet de l'orientation des fibres à l'échelle de la structure. Ph.D. Thesis, Université Paris-Est, Paris, France, 2016.
22. Matthews, F.L.; Davies GA, O.; Hitchings, D.; Soutis, C. *Finite Element Modelling of Composite Materials and Structures*; Elsevier: Amsterdam, The Netherlands, 2000.
23. Gontero, R. Modélisation du Comportement Mécanique des Structures en Bétons Fibrés à Ultra-Hautes. Ph.D. Thesis, Université de Toulouse, Toulouse, France, 2022.
24. Chen, L.; Sun, W.; Chen, B.; Shi, Z.; Lai, J.; Feng, J. Multiscale study of fibre orientation effect on pullout and tensile behavior of steel fibre reinforced concrete. *Constr. Build. Mater.* **2021**, *283*, 122506. [CrossRef]
25. Khan, Q.U.Z.; Ali, M.; Ahmad, A.; Raza, A.; Iqbal, M. Experimental and finite element analysis of hybrid fiber reinforced concrete two-way slabs at ultimate limit state. *SN Appl. Sci.* **2021**, *3*, 73. [CrossRef]
26. Huo, L.; Bi, J.; Zhao, Y.; Wang, Z. Constitutive model of steel fiber reinforced concrete by coupling the fiber inclining and spacing effect. *Constr. Build. Mater.* **2021**, *280*, 122423. [CrossRef]
27. Buratti, N.; Ferracuti, B.; Savoia, M. Concrete crack reduction in tunnel linings by steel fibre-reinforced concretes. *Constr. Build. Mater.* **2013**, *44*, 249–259. [CrossRef]
28. El-Khatib, A.; Assaad, J.J. Flexural shear strengths of structural concrete containing plastic wastes styrene–butadiene rubber latex. *Int. J. Civ. Eng.* **2022**, *20*, 967–979. [CrossRef]
29. Soetens, T.; Matthys, S. Different methods to model the post-cracking behaviour of hooked-end steel fibre reinforced concrete. *Constr. Build. Mater.* **2014**, *73*, 458–471. [CrossRef]
30. Głodkowska, W.; Laskowska-Bury, J. Proposition for Determining the Residual Strength of Fiber-Reinforced Cement Composite. *Materials* **2022**, *15*, 7546. [CrossRef]
31. Castaldo, P.; Gino, D.; Marano, G.C.; Mancini, G. Aleatory uncertainties with global resistance safety factors for non-linear analyses of slender reinforced concrete columns. *Eng. Struct.* **2022**, *255*, 113920. [CrossRef]
32. Chen, J.; Ren, X.; Feng, D.-C.; Kohler, J.; Sørensen, J.D.; Wu, J.-Y.; Le, J.-L.; Caspeele, R. Recent developments in mechanical and uncertainty modelling of concrete. *Struct. Saf.* **2024**, *113*, 102526. [CrossRef]
33. Ghanem, R.G.; Spanos, P.D. *Stochastic Finite Elements: A Spectral Approach*; Courier Corporation: North Chelmsford, MA, USA, 2003.

34. Rossi, P.; Wu, X.; Liao, F.; Huang, Z.; Yue, L.L.; Taerwe, L.; Ng, P.-L.; Kwan, A.K.-H. Probabilistic model for material behaviour analysis and appraisement of concrete structures. *Mag. Concr. Res.* **1992**, *44*, 271–280. [CrossRef]
35. Ghannoum, M.; Abdelkhalek, L.; Assaad, J.J. Application of Stochastic Finite Element Modeling to Reinforced Lightweight Concrete Beams Containing Expanded Polystyrene Beads. *Buildings* **2023**, *13*, 2294. [CrossRef]
36. Abbas, Y.M. Shear behavior of ultra-high-performance reinforced concrete beams–Finite element and uncertainty quantification study. In *Structures*; Elsevier: Amsterdam, The Netherlands, 2023; Volume 47, pp. 2365–2380.
37. Ponsi, F.; Bassoli, E.; Buratti, N.; Vincenzi, L. Parameter estimation and uncertainty quantification of a fiber-reinforced concrete model by means of a multi-level Bayesian approach. *Constr. Build. Mater.* **2024**, *438*, 136994. [CrossRef]
38. de Larrard, T.; Colliat, J.; Benboudjema, F.; Torrenti, J.; Nahas, G. Effect of the Young modulus variability on the mechanical behaviour of a nuclear containment vessel. *Nucl. Eng. Des.* **2010**, *240*, 4051–4060. [CrossRef]
39. Stefanou, G. The stochastic finite element method: Past, present and future. *Comput. Methods Appl. Mech. Eng.* **2009**, *198*, 1031–1051. [CrossRef]
40. Zhang, H.; Huang, Y.-J.; Yang, Z.-J.; Guo, F.-Q.; Shen, L.-H. 3D meso-scale investigation of ultra high performance fibre reinforced concrete (UHPFRC) using cohesive crack model and Weibull random field. *Constr. Build. Mater.* **2022**, *327*, 127013. [CrossRef]
41. Jabbour, R.; Assaad, J.J.; Hamad, B. Cost-to-performance assessment of polyvinyl alcohol fibers in concrete structures. *Mech. Adv. Mater. Struct.* **2022**, *29*, 2973–2983. [CrossRef]
42. Khayat, K.H.; Assaad, J.J. Measurement systems for determining formwork pressure of highly-flowable concrete. *Mater. Struct.* **2007**, *41*, 37–46. [CrossRef]
43. Nciri, M.; Notta-Cuvier, D.; Lauro, F.; Chaari, F.; Maalej, Y.; Zouari, B. Viscoelastic–viscoplastic model for short-fiber-reinforced composites with complex fiber orientation. *Mech. Adv. Mater. Struct.* **2019**, *26*, 842–853. [CrossRef]
44. Mardani, A.; Şahin, H.G.; Kaya, Y.; Mardani, N.; Assaad, J.J.; El-Hassan, H. Enhancing strength and durability of recycled fine aggregate mixtures using steel fibers, silica fume, and latex polymers. *Dev. Built Environ.* **2025**, *21*, 100599. [CrossRef]
45. *ASTM C469/C469M-14*; Standard Test Method for Static Modulus of Elasticity and Poisson's Ratio of Concrete in Compression. Annual Book of ASTM Standards. ASTM International: West Conshohocken, PA, USA, 2014.
46. *ASTM C642-13*; Standard Test Method for Density, Absorption, and Voids in Hardened Concrete. Annual Book of ASTM Standards. ASTM International: West Conshohocken, PA, USA, 2013.
47. *ASTM C39/C39M-18*; Standard Test Method for Compressive Strength of Cylindrical Concrete Specimens. Annual Book of ASTM Standards. ASTM International: West Conshohocken, PA, USA, 2018.
48. *ASTM C78/C78M-18*; Standard Test Method for Flexural Strength of Concrete (Using Simple Beam with Third-Point Loading). Annual Book of ASTM Standards. ASTM International: West Conshohocken, PA, USA, 2018.
49. Assaad, J.J.; Issa, C.A. Effect of recycled acrylic-based polymers on bond stress-slip behavior in reinforced concrete structures. *J. Mater. Civ. Eng.* **2017**, *29*, 04016173. [CrossRef]
50. El Mir, A.; Nehme, S.G.; Assaad, J.J. Durability of self-consolidating concrete containing natural waste perlite powders. *Heliyon* **2020**, *6*, e03165. [CrossRef] [PubMed]
51. Truong, G.T.; Choi, K.-K. Tensile behavior of hybrid composites of carbon fibers—Steel wire mesh reinforced polymer. *Mech. Adv. Mater. Struct.* **2021**, *28*, 154–166. [CrossRef]
52. Zéhil, G.-P.; Assaad, J.J. Feasibility of concrete mixtures containing cross-linked polyethylene waste materials. *Constr. Build. Mater.* **2019**, *226*, 1–10. [CrossRef]
53. Soutsos, M.; Le, T.; Lampropoulos, A. Flexural performance of fibre reinforced concrete made with steel and synthetic fibres. *Constr. Build. Mater.* **2012**, *36*, 704–710. [CrossRef]
54. Jahami, A.; Dayaa, L.; Assaad, J.J.; Baalbaki, O.; Khatib, J. Flexural Strength of Structural Beams Cast Using Combined Normal-Weight and Lightweight Concrete Mixtures. *Buildings* **2024**, *14*, 3787. [CrossRef]
55. Raad, D.; Assaad, J.J. Structural properties of fiber-reinforced concrete containing thermosetting polymer plastic wastes. *J. Sustain. Cem. Mater.* **2021**, *11*, 137–147. [CrossRef]
56. CEA. Description of the Finite Element Code Cast3m. 2015. Available online: http://www-cast3m.cea.fr/ (accessed on 1 January 2025).
57. Mazars, J. A description of micro- and macroscale damage of concrete structures. *Eng. Fract. Mech.* **1986**, *25*, 729–737. [CrossRef]
58. Giry, C.; Dufour, F.; Mazars, J. Stress-based nonlocal damage model. *Int. J. Solids Struct.* **2011**, *48*, 3431–3443. [CrossRef]
59. Breysse, D. Numerical study of the effect of inhomogeneities and boundary conditions on the tensile strength of concrete. *Mater. J.* **1991**, *88*, 489–498.
60. Van Vliet, M.R.; Van Mier, J.G. Experimental investigation of size effect in concrete and sandstone under uniaxial tension. *Eng. Fract. Mech.* **2000**, *65*, 165–188. [CrossRef]
61. Syroka-Korol, E.; Tejchman, J.; Mróz, Z. FE calculations of a deterministic and statistical size effect in concrete under bending within stochastic elasto-plasticity and non-local softening. *Eng. Struct.* **2013**, *48*, 205–219. [CrossRef]
62. Metropolis, N.; Ulam, S. The monte carlo method. *J. Am. Stat. Assoc.* **1949**, *44*, 335–341. [CrossRef] [PubMed]

63. Bouhjiti, D.-M.; Baroth, J.; Briffaut, M.; Dufour, F.; Masson, B. Statistical modeling of cracking in large concrete structures under Thermo-Hydro-Mechanical loads: Application to Nuclear Containment Buildings. Part 1: Random field effects (reference analysis). *Nucl. Eng. Des.* **2018**, *333*, 196–223. [CrossRef]
64. Ghannoum, M.; Baroth, J.; Millard, A.; Rospars, C. Stochastic finite element modeling of heterogeneities in massive concrete and reinforced concrete structures. *Int. J. Numer. Anal. Methods Géoméch.* **2024**, *48*, 1227–1244. [CrossRef]

Disclaimer/Publisher's Note: The statements, opinions and data contained in all publications are solely those of the individual author(s) and contributor(s) and not of MDPI and/or the editor(s). MDPI and/or the editor(s) disclaim responsibility for any injury to people or property resulting from any ideas, methods, instructions or products referred to in the content.